An All-Liquid-Crystal Strategy for Fast Orbital Angular Momentum Encoding and Optical Vortex Steering

Rui Yuan, Yuan Liu, Qinggui Tan, Jinman Ge, Peng Chen ⦾, Qi Guo, and Wei Hu ⦾

Abstract—An all-liquid-crystal device for fast orbital angular momentum encoding and optical vortex beam steering is proposed and demonstrated. It is a combination of a cascaded spin-determined beam deflector and an optical vortex generator. The fast switching derives from the rapid in-plane optical axis rotation of ferroelectric liquid crystal half-wave plates, while the q-plate and meta-q-plate made by photopatterned liquid crystal polymer ensure high-quality and efficient orbital angular momentum encoding. By programing the binary signals applied to the half-wave plates, electrical optical vortex deflection and 32 different orbital angular momentum encoding are achieved faster than 70 μs with a total efficiency over 85%. It supplies a practical strategy for fast optical vortex steering and orbital angular momentum encoding and may be broadly used in vortex LiDAR, multitarget communications and orbital angular momentum multiplexed optical telecoms.

Index Terms—Circular polarization, laser beam steering, laser radar, liquid crystal devices.

I. INTRODUCTION

COMPARED to radars, LiDAR exhibits superiorities such as high spatial resolution, high directionality, fast detection, excellent anti-jamming performance and light weight [1]–[3]. With its rapid development, LiDAR has achieved many applications in autonomous vehicles, unmanned drone aircraft, medical measurement, environmental and ecological monitoring, military affairs, smart cities and AR/VR [3]–[9]. The plane output wave of LiDAR leads to a weak signal reflection from oblique surfaces, thus limiting its sensitivity. This problem can be perfectly solved by adopting a vortex beam, which carries

Rui Yuan, Yuan Liu, Peng Chen, and Wei Hu are with the National Laboratory of Solid State Microstructures, College of Engineering and Applied Sciences, Nanjing University, Nanjing 210023, China (e-mail: ruiyuanedu@163.com; 13585173916@163.com; chenpeng@nju.edu.cn; huwei@nju.edu.cn).

Qinggui Tan and Jinman Ge are with the National Key Laboratory of Science and Technology on Space Microwave, China Academy of Space Technology, Xi'an 710100, China (e-mail: uestctqg@163.com; gejm@cast504.com).

Qi Guo is with the School of Instrumentation and Optoelectronic Engineering, Beihang University, Beijing 100191, China (e-mail: qguo@buaa.edu.cn).

orbital angular momentum (OAM) and has a helical phase front twisting along its propagation axis. The geometric feature of a vortex can be depicted by topological charge m, meaning the number of phase windings in a single wavelength. In other words, m reveals the velocity of the phase rotation around its axis of propagation [10]. The helical phase structure enables more scattering information to be captured with respect to plan waves; thus, the optical vortex (OV) shows great potential in ultrasensitive range detection and imaging [11]. Meanwhile, by measuring the rotational Doppler shift of the $\pm m$ OAM superposition of an OV, one can detect the rotational property of an object [12]. High-quality OAM encoding and fast nonmechanical OV steering are vital requirements for the above applications. It is an urgent pursuit to exploit compact, stable and cost-effective solutions to replace traditional mechanical steering techniques.

To date, many strategies have been developed for optical vortex generation. Liquid crystal (LC) based approaches are especially attractive due to their dynamic functions [13]–[15]. Unfortunately, the response time of common LCs is restricted to milliseconds. Overdriving can speed up the response in the electric driven process, while relaxation still suffers from a slow response due to the intrinsic elastic and viscosity limitations of LCs, severely hindering its applications. To improve the speed, fast responsive LCs such as dual-frequency LCs [16], [17] and polymer-stabilized blue phase LCs [18], [19] are patterned aligned or driven for optical vortex generation; unfortunately, the response is still limited to the submillisecond scale. Ferroelectric LC (FLC) is over two orders faster than common nematic LCs [20], [21] and thus is a promising candidate for fast OAM encoding and OV steering. However, due to the intrinsic self-organization and high viscosity of FLCs, it is challenging to accomplish high-resolution alignments, and scattering loss is inevitable, drastically degrading both the quality and efficiency of generated optical vortices [22]. Considering that conjugated phase profiles are encoded to light with orthogonal circular polarizations by the same geometric phase element, switching between conjugated phases can be achieved via spin conversion. In our previous work, a fast switch between two OVs with opposite OAMs was demonstrated based on the rapid spin conversion of an FLC waveplate [23]. However, fast multi-OAM encoding and large-range OV steering by combining the rapid polarization conversion of FLC half-wave plates and the high-quality and efficient beam shaping of traditional LCs or LC polymers has remained formidable.
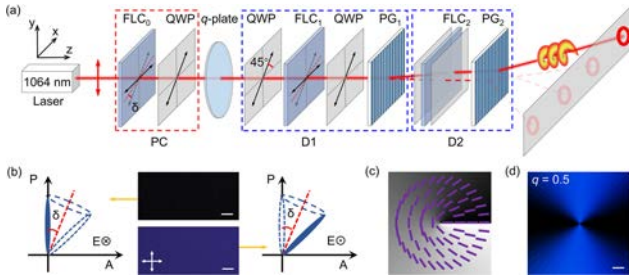
Fig. 1. (a) Optical setup for fast optical vortex beam steering. FLC_0, FLC_1 and FLC_2 are three FLC half-wave plates; PG1 and PG2 are two polarization gratings. (b) Dependencies of FLC directors on voltage polarities: left, minus 0; right, plus 1. Corresponding textures are exhibited in the middle, and P and A reveal the directions of the polarizer and analyzer, respectively. (c) Spatial director (purple bars) and geometric phase (grayscale image, black to white indicates 0 to 2π) distributions (simulated by MATLAB). (d) POM micrograph of q-plate with $q = 0.5$. All scale bars indicate 100 μm. The white arrows reveal the directions of crossed polarizers.

In this work, an all-LC strategy is proposed for high quality OAM encoding and fast OV steering. An LC polymer quarter-wave plate/FLC half-wave plate/LC polymer quarter-wave plate sandwiched element acts as a fast spin convertor. Following a polarization grating, an electrically switchable deflector is formed. By cascading a series of such modules, 1-dimensional (1D) and 2D beam steering can be obtained. Putting a q-plate in front of the cascaded deflectors, fast steering of the OV is demonstrated. While putting a meta-q-plate [24] behind the same deflector, fast OAM encoding could be achieved. This design separates the functions of dynamic switching and beam shaping and supplies a strategy for OV encoding and steering with merits of excellent beam quality, fast response and high efficiency.

II. PRINCIPLE AND EXPERIMENT

The proposed device consists of two different parts: a spin-determined beam deflector (D) and an OV generator. The beam deflector is composed of a polarization converter (PC) and a polarization grating. As illustrated by the blue frame marked D1 in Fig. 1(a), PC is a set of quarter-wave plates/half-wave plates/quarter-wave plates. The fast axes of two quarter-wave plates are parallel to each other, while the half-wave plate is an active element with an in-plane switchable fast axis (0° and 45° with respect to those of quarter-wave plates). The circular polarization conversion progress can be calculated by Jones matrix multiplication as

$$\mathbf{E}_{out} = \mathbf{J}_{QWP}\mathbf{J}_{FLCHWP}\mathbf{J}_{QWP}\mathbf{E}_{in}$$

$$= \begin{bmatrix} 1 & -i \\ -i & 1 \end{bmatrix} \begin{bmatrix} \cos(2t) & \sin(2t) \\ \sin(2t) & -\cos(2t) \end{bmatrix} \begin{bmatrix} 1 & -i \\ -i & 1 \end{bmatrix} \begin{bmatrix} 1 \\ +i \end{bmatrix}$$

$$= \begin{cases} \begin{bmatrix} 1 \\ -i \end{bmatrix}, t = 0 \\ -i \begin{bmatrix} 1 \\ +i \end{bmatrix}, t = 45° \end{cases}, \tag{1}$$

where $\mathbf{J}_{QWP}$ and $\mathbf{J}_{FLCHWP}$ are the Jones matrices [25] of the quarter-wave plate and half-wave plate, respectively; $\mathbf{E}_{in}$ indicates the left circular polarization incidence; and t is the fast axis angle of the half-wave plate with respect to the x-axis. For right

circular polarization, similar circular polarization conversion can be achieved via optical axis switching of the half-wave plate. The polarization grating is considered a patterned half-wave plate with a director following this equation in the x-y plane: $\alpha(x) = -\pi x/\Lambda$, where Λ is the period of the polarization grating. It works as a circular polarization-dependent beam splitter and diffracts orthogonal circular polarization components to $\pm 1^{st}$ order. Therefore, the input light can be completely switched between $\pm 1^{st}$ orders by flipping incident spins (circular polarizations) [26]. The diffraction angle χ satisfies the grating equation $\chi = \sin^{-1}(\lambda/\Lambda)$, where λ is the incident wavelength. This means that χ can be precisely tuned by presetting Λ. Thus, the function of the spin-determined beam deflector is realized. Through cascading such beam deflectors and optimizing the Λ of each polarization grating, beams could be electrically addressed among a matrix.

Q-plate plays as the OV generator. It is a geometric phase optical element with a space-variant optical axis depicted by $\beta = q\varphi + \beta_0$, where q is the topological charge, φ is the azimuthal angle, and β_0 is the initial orientation when $\varphi = 0$ and is assumed to be zero here [27]. When a circularly polarized plane wave passes through the q-plate, the beam carries a topological charge of $2q$ with a spin-dependent sign. Meanwhile, the output spin is inverted. Simply combing the above two parts, beam steering on the objective OV can be obtained. If a meta-q-plate with different q exactly located on separate lattice points is adopted, OAM encoding can be arbitrarily implemented. Additionally, the q-plate and meta-q-plate show similar spin dependencies to polarization gratings. The sign of the generated OAM can be inverted via spin flipping.

Here, an active half-wave plate with an in-plane switchable fast axis is accomplished on the basis of the electrically suppressed helix mode of FLC (FD4004N, DIC Co., Japan). Photoalignment agent SD1 (DIC Co., Japan), whose absorption oscillators tend to reorient perpendicularly to illuminated polarization, is used to carry out all alignments [28]. When the polarity of the voltage is applied to the homogenous FLC half-wave plate altering, the FLC directors are switched by $\pm\delta$ around the alignment direction (red dotted line in Fig. 1(b)). Herein, $\delta = 22.05°$ [29] leads to a small deviation of optical axis rotation 2δ (44.1°) to 45°. As shown in Fig. 1(b), uniform phase retardation is observed under a polarized optical microscope (POM). The mechanism for circular polarization conversion here is distinguished from traditional nematic variable phase retarders, which electrically change the tilt angle to switch the phase retardance between 0 and π and thus convert the spins accordingly. In this work, the same function is realized by a set of quarter-wave plates /FLC half-wave plates/quarter-wave plates. LC polymer (UCL-P100, DIC Co., Japan) with optimized thickness is unidirectionally aligned and polymerized under UV to form quarter-wave plates for target wavelength $\lambda = 1064$ nm. Then, these quarter-wave plates are removed from the glass substrate by an optically clear adhesive film (OCA, 8173D, 3 M, USA) [30] and transferred to the FLC half-wave plate to form the PC. The thickness of each quarter-wave plate is ~ 2 μm, making a single retarder still integrated. The director distribution of a q- plate with $q = 0.5$ as shown in Fig. 1(c), is recorded by a digital micromirror device-based microlithography setup
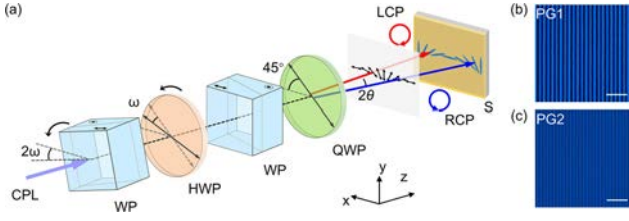
Fig. 2. (a) Schematic illustration of a polarization hologram setup based on rotatable dual Wollaston prisms. Dark arrows represent the local linear polarization direction; blue bars represent corresponding LC directors; S: sample coated with SD1. POM micrographs of (b) PG1 and (c) PG2. All scale bars indicate 20 μm.

[31]. In Fig. 1(d), the color variation under POM reveals the continuous change of the LC director from 0 to 180°.

The polarization gratings are fabricated by polarization holography with a rotatable dual Wollaston prism setup (Fig. 2(a)) [32]. Here, dual Wollaston prisms are used to separate two orthogonal linear polarized components to a certain angle (2θ). The angle can be continuously tuned by changing the angle between two Wollaston prisms (2ω). To keep the polarizations parallel to the optical axes of WP, a half-wave plate is rotated by ω accordingly. A quarter-wave plate is aligned to convert the two linearly polarized components to orthogonal circular polarizations. The interference between the orthogonal circular polarizations will induce a vector field with periodically and continuously changed linear polarization with uniform intensity. After recording this polarization information, the SD1 film will transfer the order to the coated LC polymer. The period of polarization grating Λ is determined by [33]:

$$\Lambda = \frac{\lambda_R}{2 \sin(\theta)}, \tag{2}$$

where λ_R is the recording wavelength and θ is half of the beam separation angle. Fig. 2(b) and 2(c) present two polarization gratings with periods of 4.0 μm and 8.0 μm, respectively. In our experiments, PG1 with a larger Λ is placed near the laser to reduce the influence caused by oblique incidence.

The light source is a 1064 nm laser. Diffraction patterns are captured by a charge coupled device (CCD), and intensities are detected with a power meter (Newport-1930c). The astigmatic transformation method [34] is adopted by inserting a cylindrical lens ($f = 100$ mm) in front of the CCD and capturing the converted pattern at its focal plane, to verify the topological charge of OVs.

III. RESULTS AND DISCUSSION

A. 1 × 4 OV Beam Steering

We cascade two deflectors with different Λ of polarization gratings (4.0 μm and 8.0 μm) to form a 1 × 4 OV deflector. A q-plate with $q = 0.5$ is adopted for OV generation. The optical setup is exactly the same as that presented in Fig. 1(a). FLC_0, FLC_1 and FLC_2 are only active elements in the setup. As shown in Fig. 3(a), the generated OV can be electrically addressed among four diffraction orders ($\pm 1^{st}$ and $\pm 2^{nd}$) by programing the binary signal applied to FLC_1 and FLC_2. Their diffraction angles are $\pm 7.6°$ and $\pm 23.5°$, respectively. Altering the binary
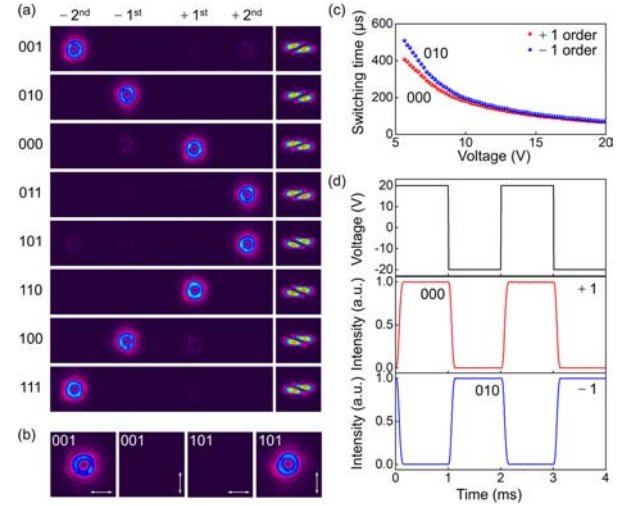

Fig. 3. (a) OV positions (left) and corresponding detected OAMs (right) dependent on binary signal applied to different FLC half-wave plates. (b) Dependency of output polarization on binary signals applied to different FLC half-wave plates with corresponding labeled signals. Arrows indicate directions of analyzers. (c) The dependency of switching time on applied voltage. (d) Waveform of a 500 Hz square wave (top) with a driving voltage of 20 V. Switching responses of $+1^{st}$ order (middle) and -1st order (bottom).

signal applied to FLC_0 causes the flipping of the sign of OAM, as verified by the detection. In these CCD captured images, different colors are utilized to record the intensity distribution of the invisible 1064 nm laser. As mentioned above, polarization gratings and cascaded polarization gratings work as circular polarization splitters, and thus, left/right circular polarizations are deflected to opposite sides of the propagation axis. Here, a quarter-wave plate aligned $-45°$ to the x-axis is utilized to convert the circular polarization to linear polarization for detection. Beams after 001 (each bit corresponds to the binary signal applied to FLC from left to right in Fig. 1(a)) and 101 signal applied systems are measured with horizontally and vertically placed polarizers separately, and the results shown in Fig. 3(b) verify the above expectation.

The speed of OV beam steering is determined by the response of FLC half-wave plates. All the FLC half-wave plates are optimized for a 1064 nm incident wavelength and exhibit excellent consistency. We choose the switching between 010 and 000 states, *i.e.*, the switching of electrically suppressed helix mode of FLC_1, as an example. With increasing applied voltage, the switching time decreases significantly, as shown in Fig. 3(c). We define the switching time as the duration of intensity change between 10% and 90%. When 20 V is applied to the FLC half-wave plate, the switching times corresponding to the 000 and 010 states are 67 μs and 69 μs, respectively (Fig. 3(d)). Because simple segmented electrodes are adopted, it is convenient to supply high voltage with an amplifier. The fast response superiority of FLC is thus fully exhibited here.

It needs to be mentioned that the OV steering is discrete here. This issue could be addressed by further introducing an optical phase array as a fine scanning module to accomplish a quasi-continuous deflection between adjacent orders [35]. The cascaded deflectors here drastically extend the detection range of vortex LiDAR without reducing the spatial resolution.
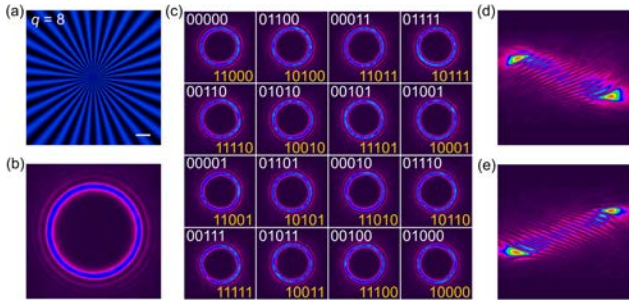
Fig. 4.   (a) Micrograph of q-plate with $q = 8$. Scale bar indicates 100 μm. (b) Generated OV with $m = 16$. (c) 4×4 OV matrix with position dependent binary signals. White and yellow numbers are related to orthogonal incident circular polarizations. (d) and (e) the detected OAMs of $m = \pm 16$.

B. 4×4 OV Beam Steering

We cascade another two deflectors orthogonally to form a 4×4 OV deflector. To reduce the influence of oblique incidence, the four deflectors are alternately placed with larger Λ deflectors put ahead. With a q-plate of $q = 8$ (Fig. 4(a)), OV of $m = 16$ is generated (Fig. 4(b)). As shown in Fig. 4(c), the generated OV can be electrically addressed among the 4×4 matrix by programing binary signals applied to five respective FLC half-wave plates (FLC$_0$, FLC$_1$, FLC$_2$, FLC$_3$ and FLC$_4$). This means that each lattice point is connected to two series of binary signals, and the difference between them is the opposite sign of OAM, as presented in Fig. 4(d) and 4(e). The number of lattice points equals 2^n, where n is the number of deflector modules. Introducing more such modules, the matrix can be significantly extended. This may significantly extend the detection range of vortex LiDAR.

C. 4×4 Fast OAM Encoding

In addition to vortex beam steering, fast encoding on OAM is also a key requirement. Different OAM modes are inherently orthogonal and thus can be adopted as separate channels and quantum states in OAM-based optical communications [36], [37] and quantum optics [38], [39]. OAM multiplexing adds a practical method for terabit data transmission [37], [40], [41]. The new dimension is beneficial for multiplexed free space optical links and radar imaging [11], [42], [43]. Multiple OAMs can increase azimuthal resolution without motion limitations in the target detection and imaging.

We put a meta-q-plate, with q continuously changing from 0.5 to 8 with an interval of 0.5 (Fig. 5(a)), one to one correspondence to the 4×4 matrix of deflection orders. It enables an electrically controlled OAM encoding. A plane wave passes through the cascaded deflectors first, with which the beam could be deflected among a 4×4 matrix, and then encodes an OAM by one q-plate unit once. All predefined topological charges could be encoded by properly programing a series of binary signals to deflect the beam to the corresponding q-plate unit, as shown in Fig. 5(b). It needs to be mentioned that the generated OAM of OVs is $2q$. Further introducing a PC altered the sign of OAM (Fig. 5(c) and (d)). If the incident beam is an OV with a certain m, the same device will act as an OAM adder, leading to an OAM variation of $\pm 2q$.
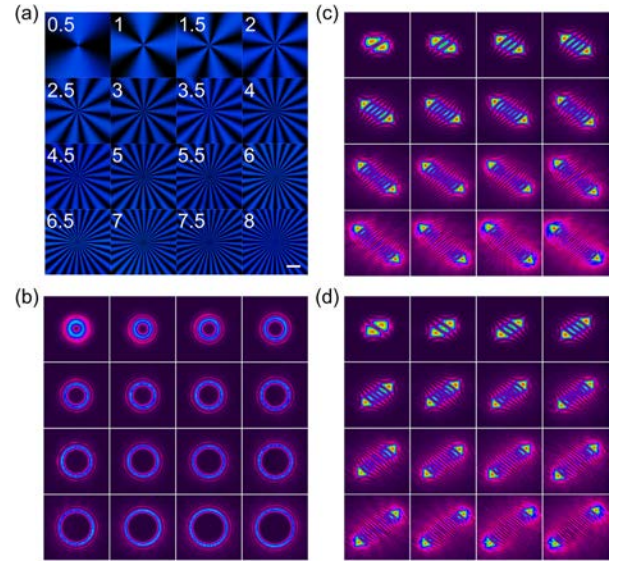

Fig. 5.   (a) Meta-q-plate with q continuously changing from 0.5 to 8 with an interval of 0.5. Scale bar indicates 100 μm. (b) Matrix of all generated OVs corresponding to the meta-q-plate. (c), (d) Detected OAMs with opposite signs.

The proposed all-LC concept successfully divides the dynamic switching and beam shaping functions. This design makes full use of the fast response superiority of FLC and completely avoids its shortcomings in patterning. With the polarity variation of applied voltages (20 V), the switching among different lattice points reaches <70 μs. It is 2~3 orders faster than traditional nematic LCs and permits fast OV steering and OAM encoding over 5 kHz. Since beam shaping is realized by photopatterned LC polymers, high resolution and efficiency are easily achieved. The diffraction efficiency is defined as the intensity of the objective OV beam divided by the total transmittance. The efficiencies of PG1 and PG2 reach 99.3% and 97.1%, respectively. The efficiency of the all-LC device exceeds 85.6%. The deviation is attributed to two reasons: one is the polarization-dependent loss caused by the slight mismatch of quarter-wave plates and half-wave plates, the discrepancy between real and ideal t and phase retardation deviation induced by oblique incidence; the other is scattering loss from microstructures and material nonuniformity. The efficiency is improvable via material and process optimizations. In addition to OVs, other structured optical fields could be obtained. This work provides a versatile strategy for fast tailoring wavefronts, which may upgrade present dynamic optics.

IV. CONCLUSION

We proposed a compact, stable and cost-effective all-LC strategy to replace traditional mechanical steering techniques by cascading spin determined beam deflectors and OV generators that separate the dynamic switching and beam shaping functions and demonstrated its utilization in fast OV steering and OAM encoding. Through programing the binary signals applied to the FLC half-wave plates, OVs were electrically addressed among the designed matrix and encoded with different OAMs. In addition to fast electrically vortex beam steering, 32 separate OAMs are encoded simultaneously. The switching time of 70 μs derived from the rapid in-plane optical axis rotation of FLC half-wave

plates is 2 orders of magnitude faster than traditional nematic LC retarders [20], [21], significantly faster than dual-frequency LCs [16], [17] and blue phases [18], [19]. Meanwhile, the quarter-wave plates, *q*-plate, meta-*q*-plate and PGs are all made by photopatterned LC Polymer, the high resolution permitting efficient OAM encoding in excellent beam quality. The efficiencies of PGs reach over 97.1%, and the total efficiency is over 85%. It supplies a practical and versatile strategy for high-quality beam shaping and fast steering, and may inspire advanced optical applications in LiDAR, OAM-multiplexed optical telecoms and links.

ACKNOWLEDGMENT

REFERENCES

[1] D. Onori, F. Laghezza, F. Scotti, M. Scaffardi, and A. Bogoni, "Coherent radar/lidar integrated architecture," in *Proc. Eur. Radar Conf.*, 2015, pp. 241–244.

[2] H. Guan, W. Yan, Y. Yu, L. Zhong, and D. Li, "Robust traffic-sign detection and classification using mobile LiDAR data with digital images," *IEEE J. Sel. Topics Appl. Earth Observ. Remote Sens.*, vol. 11, no. 5, pp. 1715–1724, May 2018.

[3] J. Liu, Q. Sun, Z. Fan, and Y. Jia, "TOF lidar development in autonomous vehicle," presented at *IEEE 3rd Optoelectron. Glob. Conf.*, Shenzhen, China, Nov. 2018, pp. 185–190.

[4] P. Qi, X. Zhao, and R. Palacios, "Autonomous landing control of highly flexible aircraft based on lidar preview in the presence of wind turbulence," *IEEE Trans. Aerosp. Electron. Syst.*, vol. 55, no. 5, pp. 2543–2555, Jan. 2019.

[5] S. F. Ramadhan, M. Taufik, D. Novita, and A. Turnip, "Design of 2D LiDar-based indoor SLAM for medical robot Covid-19," in *Proc. Int. Conf. Artif. Intell. Mechatronics Syst.*, 2021, pp. 1–5.

[6] Y. Zhu *et al.*, "Retrieving the vertical distribution of PM2.5 mass concentration from lidar via a random forest model," *IEEE Trans. Geosci. Remote.*, to be published, doi: 10.1109/TGRS.2021.3102059.

[7] B. Lv *et al.*, "LiDAR-enhanced connected infrastructures sensing and broadcasting high-resolution traffic information serving smart cities," *IEEE Access*, vol. 7, pp. 79895–79907, Jun. 2019.

[8] A. Y. Tychkov, A. V. Grachev, and A. K. Alimuradov, "Virtual reality in information transfer," in *Proc. Int. Russian Automat. Conf.*, 2020, pp. 826–830.

[9] L. Kai, L. Jun-Jie, W. Jing, and W. Xiao-Jun, "Research on augmented reality technology of helicopter aided navigation based on lidar," in *Proc. IEEE 7th Int. Conf. Virtual Reality*, 2021, pp. 373–379.

[10] A. A. Kovalev and V. V. Kotlyar, "Propagation-invariant laser beams with an array of phase singularities," *Phys. Rev. A*, vol. 103, no. 6, 2021, Art. no. 063502.

[11] K. Liu *et al.*, "Super-resolution radar imaging based on experimental OAM beams," *Appl. Phys. Lett.*, vol. 110, no. 16, Feb. 2017, Art. no. 164102.

[12] S. Murali *et al.*, "Volumetric capacitance of compressed activated microwave-expanded graphite oxide (a-MEGO) electrodes," *Nano Energy*, vol. 2, no. 5, pp. 764–768, Aug. 2013.

[13] Z. k. Zhu, K. Huang, H. z. Zhang, and J. g. Lu, "Multi-wavelength and bandwidth tunable liquid crystal filter," *Chin. J. Liq. Cryst. Disp.*, vol. 36, no. 4, pp. 516–521, Apr. 2021.

[14] Y. J. Wang, H. A. Hsieh, and Y. H. Lin, "Electrically tunable gradient-index lenses via nematic liquid crystals with a method of spatially extended phase distribution," *Opt. Exp.*, vol. 27, no. 22, pp. 32398–32408, Oct. 2019.

[15] Y. J. Wang, Y. H. Lin, O. Cakmakci, and V. Reshetnyak, "Polarization aberrations of electrically tunable liquid crystal mirrors," *Opt. Exp.*, vol. 28, no. 8, pp. 11356–11371, Apr. 2020.

[16] W. Duan *et al.*, "Helicity-dependent forked vortex lens based on photo-patterned liquid crystals," *Opt. Exp.*, vol. 25, no. 13, pp. 14059–14064, Jun. 2017.

[17] O. Melnyk *et al.*, "Fast switching dual-frequency nematic liquid crystal tunable filters," *ACS Photon.*, vol. 8, no. 4, pp. 1222–1231, Apr. 2021.

[18] S. J. Ge *et al.*, "Optical array generator based on blue phase liquid crystal Dammann grating," *Opt. Mater. Exp.*, vol. 6, no. 4, pp. 1087–1092, Apr. 2016.

[19] K. Goda, I. Watanabe, E. Fukuda, and K. Takatoh, "Fast response polymer stabilized blue phase by overdrive technique," *Jpn. J. Appl. Phys.*, vol. 59, no. 1, Jan. 2020, Art. no. 014003.

[20] Z. B. Sun, Z. N. Yuan, A. Nikita, H. S. Kwok, and A. K. Srivastava, "Fast-switchable, high diffraction-efficiency ferroelectric liquid crystal fibonacci grating," *Opt. Exp.*, vol. 29, no. 9, pp. 13978–13986, Apr. 2021.

[21] S. Mukherjee *et al.*, "Fast refocusing lens based on ferroelectric liquid crystals," *Opt. Exp.*, vol. 29, no. 6, pp. 8258–8267, Mar. 2021.

[22] Y. Ma *et al.*, "Fork gratings based on ferroelectric liquid crystals," *Opt. Exp.*, vol. 24, no. 6, pp. 5822–5828, Mar. 2016.

[23] Y. Liu *et al.*, "Ferroelectric liquid crystal mediated fast switchable orbital angular momentum of light," *Opt. Exp.*, vol. 27, no. 25, pp. 36903–36910, Dec. 2019.

[24] W. Ji *et al.*, "Meta-q-plate for complex beam shaping," *Sci. Rep.*, vol. 6, May 2016, Art. no. 25528.

[25] P. Yeh and C. Gu, *Optics of Liquid Crystal Displays*, New York, NY, USA: John Wiley & Sons, 1999, pp. 103–110.

[26] C. Provenzano, P. Pagliusi, and G. Cipparrone, "Highly efficient liquid crystal based diffraction grating induced by polarization holograms at the aligning surfaces," *Appl. Phys. Lett.*, vol. 89, no. 12, Sep. 2006, Art. no. 121105.

[27] L. Marrucci, C. Manzo, and D. Paparo, "Pancharatnam-berry phase optical elements for wave front shaping in the visible domain: Switchable helical mode generation," *Appl. Phys. Lett.*, vol. 88, no. 22, Art. no. 221102, May 2006.

[28] V. Chigrinov *et al.*, "Diffusion model of photoaligning in azo-dye layers," *Phys. Rev. E*, vol. 69, no. 6, Jun. 2004, Art. no. 061713.

[29] A. K. Srivastava, W. Hu, V. G. Chigrinov, A. D. Kiselev, and Y. Q. Lu, "Fast switchable grating based on orthogonal photo alignments of ferroelectric liquid crystals," *Appl. Phys. Lett.*, vol. 101, no. 3, Jul. 2012, Art. no. 031112.

[30] M. J. Tang *et al.*, "Integrated and reconfigurable optical paths based on stacking optical functional films," *Opt. Exp.*, vol. 24, no. 22, pp. 25510–25514, Oct. 2016.

[31] H. Wu *et al.*, "Arbitrary photo-patterning in liquid crystal alignments using DMD based lithography system," *Opt. Exp.*, vol. 20, no. 15, pp. 16684–16689, Jul. 2012.

[32] M. Miskiewicz *et al.*, "Progress on large-area polarization grating fabrication," in *Proc. Acquisition, Tracking, Pointing, Laser Syst. Technol. XXVI: 8395G*, Baltimore, MD, USA, 2012, pp. 1–7.

[33] T. Zhan, J. Xiong, Y. H. Lee, R. Chen, and S. T. Wu, "Fabrication of Pancharatnam-Berry phase optical elements with highly stable polarization holography," *Opt. Exp.*, vol. 27, no. 3, pp. 2632–2642, Feb. 2019.

[34] B. P. da Silva, D. S. Tasca, E. F. Galvão, and A. Z. Khoury, "Astigmatic tomography of orbital-angular-momentum superpositions," *Phys. Rev. A*, vol. 99, no. 4, Apr. 2019, Art. no. 043820.

[35] V. Marinova *et al.*, "Graphene-based spatial light modulator operating at near infrared spectral range," *Appl. Surf. Sci.*, vol. 472, pp. 2–9, Sep. 2019.

[36] T. Lei *et al.*, "Massive individual orbital angular momentum channels for multiplexing enabled by Dammann gratings," *Light-Sci. Appl.*, vol. 4, no. 3, Dec. 2015, Art. no. e257.

[37] M. Adiya, H. Kishikawa, N. Goto, and G. Shagdar, "8-ary orbital angular momentum shift keying for free-space optical communication system," *Opt. Eng.*, vol. 59, no. 2, Feb. 2020, Art. no. 026102.

[38] A. Nicolas *et al.*, "A quantum memory for orbital angular momentum photonic qubits," *Nat. Photon.*, vol. 8, no. 3, pp. 234–238, Mar. 2014.

[39] D. S. Ding *et al.*, "Quantum storage of orbital angular momentum entanglement in an atomic ensemble," *Phys. Rev. Lett.*, vol. 114, no. 5, Feb. 2015, Art. no. 050502.

[40] A. E. Willner *et al.*, "Orbital-angular-momentum-based reconfigurable optical switching and routing," *Photon. Res,* vol. 4, no. 5, pp. B5–B8, Oct. 2016.

[41] R. M. Fouda, A. Ebrahimi, T. C. Baum, and K. Ghorbani, "Experimental BER performance of quasi-circular array antenna for OAM communications," *IEEE Antennas Wireless Propag. Lett.*, vol. 19, no. 8, pp. 1350–1354, Aug. 2020.

[42] K. Liu, Y. Cheng, X. Li, and Y. Jiang, "Passive OAM-based Radar imaging with single-in-multiple-out mode," *IEEE Microw. Wireless Compon. Lett.*, vol. 28, no. 9, pp. 840–842, Sep. 2018.

[43] H. Liu, Y. Wang, J. Wang, K. Liu, and H. Wang, "Electromagnetic vortex enhanced imaging using fractional OAM beams," *IEEE Antennas Wireless Propag. Lett.*, vol. 20, no. 6, pp. 948–952, Jun. 2021.

Rui Yuan was born in Jiangsu, China, in 1992. He received the M.S. degree in physics from the Hebei University of Technology, Tianjin, China, in 2018. He is currently working toward the Ph.D. degree with the National Laboratory of Solid State Microstructures, College of Engineering and Applied Sciences, Nanjing University, Nanjing, China. His current research interests include liquid crystal based beam-steering, optical phase array, and tunable lens.

Peng Chen was born in Yangzhou, Jiangsu, China, in 1992. He received the B.S. and Ph.D. degrees in material physics and optical engineering from Nanjing University, Nanjing, China, in 2014 and 2019, respectively. From 2019 to 2021, he was a Research Associate with the College of Engineering and Applied Sciences, Nanjing University. Since 2021, he has been an Associate Professor with Nanjing University. His research interests focus on liquid-crystal-mediated geometric phase optics and their applications.

Yuan Liu was born in Jiangsu, China, in 1995. She received the B.S. degree in 2018 from the College of Engineering and Applied Sciences, Nanjing University, Nanjing, China, where she is currently working toward the Ph.D. degree. Her current research interests include the linear and nonlinear light manipulation based on liquid crystals and lithium niobate optical materials.

Qi Guo was born in Harbin, China, in 1987. She received the B.S. degree from the Department of Physics, Harbin Institute of Technology, Harbin, China, in 2008, and the Ph.D. degree from the Department of Electronic and Computer Engineering, Hong Kong University of Science and Technology, Hong Kong, in 2014. From 2014 to 2020, she was an Assistant Professor with the School of Instrumentation and Optoelectronic Engineering, Beihang University, Beijing, China. Since 2020, she has been an Associate Professor with Beihang University. Her research interests include photoalignment of ferroelectric liquid crystals, liquid crystal gratings and their applications, and liquid crystal devices.

Qinggui Tan was born in Yishui, Shandong, China, in 1975. He received the Ph.D. degrees in optical from the University of Electronic Science and Technology of China, Chengdu, China, in 2006. He is currently a Professor with the National Key Laboratory of Science and Technology on Space Microwave, CAST, Xi'an, China. His research fields are microwave photonics, space laser communication, and optical phased array antenna.

Jinman Ge was born in Jiaozuo, Henan, China, in 1984. She received the Ph.D. degrees in optical engineering from the Nanjing University of Science and Technology, Nanjing , China, in 2018. She is a Postdoctoral Fellow of the National Key Laboratory of Science and Technology on Space Microwave and works in the Xi'an Branch of the China Academy of Space Technology, China. Her research interests include space laser communication, optical phased array antennas, and optical precision measurement technology.

Wei Hu was born in Rizhao, Shandong, China, in 1981. He received the Ph.D. degree in polymer chemistry from Jilin University, Changchun, China, in 2009. He is currently a Professor of optical engineering with Nanjing University, Nanjing, China. His research interests include liquid crystal materials and optical devices, with a focus on photoalignment-enabled liquid crystalline superstructures, optically addressed spatial light modulators, and liquid crystal telecom/terahertz elements.